



Low-temperature photoluminescence spectroscopy of $\text{CH}_3\text{NH}_3\text{PbBr}_x\text{Cl}_{3-x}$ perovskite single crystals

Qiang Xu ^{a,*}, Wenyi Shao ^a, Xinlei Zhang ^a, Jun Liu ^b, Xiaoping Ouyang ^{a,b}, Xiaobin Tang ^a, Wenbao Jia ^a

^a Department of Nuclear Science and Engineering, Nanjing University of Aeronautics and Astronautics, Nanjing, 211106, China

^b Northwest Institute of Nuclear Technology, Xi'an, 710024, China

ARTICLE INFO

Article history:

Received 18 January 2019
Received in revised form
30 March 2019
Accepted 1 April 2019
Available online 5 April 2019

Keywords:

Perovskite single crystals
Temperature dependent
photoluminescence
Free exciton emission
Bound exciton emission
Phase transition

ABSTRACT

Organic-inorganic halide perovskite (OIHP) has attracted tremendous attention due to its potential applications in optoelectronics such as light emitting device and photodetector. Here, we have grown high quality $\text{CH}_3\text{NH}_3\text{PbBr}_x\text{Cl}_{3-x}$ perovskite single crystals and investigated the luminescence mechanism of these materials. The results indicate that optical properties of $\text{CH}_3\text{NH}_3\text{PbBr}_x\text{Cl}_{3-x}$ perovskite materials are strongly depend on the temperature and the dope concentration. Free exciton recombination emission has dominant contribution to luminescence spectra of materials at orthorhombic structure, as bound exciton recombination emission to the spectra of materials at cubic structure. Based on temperature-dependent photoluminescence, the exciton binding energy of $\text{CH}_3\text{NH}_3\text{PbCl}_3$ and $\text{CH}_3\text{NH}_3\text{PbBr}_{0.3}\text{Cl}_{2.7}$ are calculated as about 22.9 meV and 27.1 meV, respectively.

© 2019 Elsevier B.V. All rights reserved.

1. Introduction

Organic-inorganic hybrid perovskite (OIHP) $\text{CH}_3\text{NH}_3\text{PbX}_3$ ($X = \text{Cl}^-$, Br^- , or I^-) has been considered as the most promising material for energy conversion applications due to its unique physical and optical properties. Recently, power conversion efficiency (PCE) of perovskite solar cells reached a record of 23.2% [1]. It has shown great potential to compete with well-established silicon solar cells in terms of PCE and cost [2]. In addition, because of its band gap tunability, high color purity, high photoluminescence (PL) efficiency, and low cost synthesis methods, OIHP has been gaining extensive attention for use in other optoelectronic applications (LEDs, lasers, photodetectors, transistors) [3–6]. OIHP is also increasingly being used for ionizing radiation detection due to its strong stopping power, defect-tolerance, large mobility lifetime ($\mu\tau$) [7–10]. Pure $\text{CH}_3\text{NH}_3\text{PbCl}_3$, $\text{CH}_3\text{NH}_3\text{PbBr}_3$ and $\text{CH}_3\text{NH}_3\text{PbI}_3$ have been synthesized and fabricated as optoelectronic devices to detect UV–Visible photons or convert UV–Visible photon energy into electricity. Although single halogen perovskite crystals have

been greatly successful, there are some application limitations. To meet the requirement of various devices, growing high quality materials with tunable electrical and optical properties has attracted a lot of attention, and using mixed halide hybrid perovskite is a key strategy to overcome most application limitations [11–13]. H. Wei et al. [14] reported high quality and dopant compensated $\text{CH}_3\text{NH}_3\text{PbBr}_{3-x}\text{Cl}_x$ perovskite single crystals that enable to overcome the limitations of device noise and charge collection. The dopant-compensated $\text{CH}_3\text{NH}_3\text{PbBr}_{2.94}\text{Cl}_{0.06}$ alloy has over tenfold improvement on bulk resistivity of $3.6 \times 10^9 \Omega \text{ cm}$, which increases the hole mobility to $560 \text{ cm}^2 \text{ V}^{-1} \text{ s}^{-1}$ and the mobility–lifetime product to $1.8 \times 10^{-2} \text{ cm}^2 \text{ V}^{-1}$. Therefore, a high-resolution gamma spectrum (^{137}Cs) has been achieved at room temperature with low electrical field. Additionally, due to the introduction of chlorine, the synthetic mixed halide perovskite film ($\text{CH}_3\text{NH}_3\text{PbI}_{3-x}\text{Cl}_x$) has higher carrier mobility and much longer exciton diffusion length [15]. Wu et al. [16] demonstrated a flexible photodetector array based on $\text{CH}_3\text{NH}_3\text{PbI}_{3-x}\text{Cl}_x$ film with a resolution of 63.5 dpi for photosensing and imaging. The device possessed fine photoresponse properties with high on/off current ratio (1.2×10^3) under a light intensity of 38.3 mW cm^{-2} , high detectivity (9.4×10^{11} Jones) at a light intensity of 0.033 mW cm^{-2} . J. Hieulle et al. [17] investigated the impact of halide mixing on perovskite

* Corresponding author.

E-mail address: xuqiangxmu@nuaa.edu.cn (Q. Xu).

stability. Their results indicated that the incorporation of Cl into $\text{CH}_3\text{NH}_3\text{PbBr}_3$ leads to an increase of the decomposition energy, which makes the perovskite film more stable to external stimuli. This increase in stability is related to the stronger bond strength of Cl-Pb than Br-Pb and I-Pb. In addition, they determined the optimum Cl incorporation ratio that could provide higher stability without substantially changing the band gap of the perovskite material, pointing out an important direction for the fabrication of stable perovskite devices. It is obvious that the performance of OIHP exhibits a large variation after low ratios Cl doping into either $\text{CH}_3\text{NH}_3\text{PbBr}_3$ or $\text{CH}_3\text{NH}_3\text{PbI}_3$ crystals and films.

During the past several years, intensive efforts have been done on optoelectronics based on $\text{CH}_3\text{NH}_3\text{PbCl}_3$ SCs, but the performances of these devices are still far away from being commercially used. Br-doped $\text{CH}_3\text{NH}_3\text{PbCl}_3$ has a great potential to enhance the performances of these devices. However, the fundamental effects of Br-doped $\text{CH}_3\text{NH}_3\text{PbCl}_3$ SC on optical properties remain unresolved. Furthermore, the outstanding properties of solution-growth OIHP have also promoted the application developments. Herein, high quality $\text{CH}_3\text{NH}_3\text{PbBr}_{x}\text{Cl}_{3-x}$ perovskite SCs materials have been synthesized by using solution growth method. The structural properties of the crystals are characterized by X-ray diffraction (XRD), and home-made X-ray fluorescence (XRF) measurement. Optical properties are obtained by UV–Vis transmission spectrometer and photoluminescence measurement. The temperature-dependent photoluminescence (PL) properties of $\text{CH}_3\text{NH}_3\text{PbCl}_3$ and $\text{CH}_3\text{NH}_3\text{PbBr}_{0.3}\text{Cl}_{2.7}$ in the range of 10 K–290 K have been investigated. The phase transition is proved by the peak position and full width at half maximum (FWHM). The exciton binding energy is also calculated from the temperature-dependent PL spectra, which is a critical factor that affects the optical properties of the perovskite crystals and can be tuned by halogen doping concentration. Our research helps on understanding the temperature-controlled phase transition of photoexcited exciton and provides a theory for selecting the appropriate halide composition and temperature conditions for optoelectronics.

2. Experimental section

2.1. Materials

All the chemicals were purchased from commercial company without further purification. Methylamine (CH_3NH_2 , 33 wt% in absolute ethanol), hydrobromic acid (HBr, 48 wt% in water), lead bromide crystalline powder (PbBr_2 , 99.99%) and lead chloride crystalline powder (PbCl_2 , 99.99%) were purchased from Aladdin Reagent Co. Dimethylsulfoxide (DMSO, anhydrous, ≥99.0%); N,N-dimethylformamide (DMF, anhydrous, ≥99.5%), hydrochloride acid (HCl, 38 wt% in water), diethyl ether (anhydrous, ≥99.7%) and ethanol (anhydrous, ≥99.7%) were purchased from Nanjing Chemical Reagent Co.

2.2. Crystals growth

Synthesis of MACl powder. A molar ratio of 1.2:1 methylamine and hydrochloride acid was reacting in 0 °C by using an ice bath. After reacting for 2.5 h, the solution was evaporated at 60 °C in a rotary evaporator, and then white MACl powder was obtained. In order to improve the MACl purity, it was purified for at least three times with ethanol and diethyl ether. Finally, high purity white MACl powder was collected and stored in vacuum atmosphere with a temperature of 60 °C for 24 h.

Synthesis of $\text{CH}_3\text{NH}_3\text{PbBr}_{x}\text{Cl}_{3-x}$ single crystals. High quality $\text{CH}_3\text{NH}_3\text{PbBr}_{x}\text{Cl}_{3-x}$ perovskite SCs were grown with a solution process based on the inverse temperature crystallization method.

Various molar ratios among $\text{CH}_3\text{NH}_3\text{Cl}$, PbCl_2 and PbBr_2 were dissolved into different volume ratios between dimethylsulfoxide and N-N, by using dimethylformamide as precursor solution. Then the precursor solution was filtered using PTFE filter with 2 μm pore size and kept in oil bath at temperature of 80 °C. After several days, $\text{CH}_3\text{NH}_3\text{PbBr}_{x}\text{Cl}_{3-x}$ perovskite SCs were harvested from the solution.

2.3. Characterization

The structural properties of the material were investigated by powder X-ray diffraction (XRD) and X-ray fluorescence (XRF) spectroscopy. XRD patterns were obtained by an X-ray diffractometer (Rigaku Ultima IV diffractometer) using Cu-K α radiation ($\lambda = 0.15406 \text{ nm}$). XRF system consists of an X-ray generator, a silicon drift detector (AMPTEK Inc. Model X-123SDD, America) with 125 eV resolution at 5.9 keV that was coupled to a multichannel analyzer (AMPTEK Inc. Model DP5, America) and lase finder. The X-ray tube (Ag anode target) with 7.8 μm beryllium window was collimated by a 2 mm diameter collimator [18]. The optical transmission spectrum was recorded on a Shimadzu UV 2550 spectrophotometer at room temperature. Low temperature PL spectra were measured from 10 K to 290 K, and were collected using a spectrometer (Princeton Instruments SP2500i/SP2300i). During the measurement, the crystals were loaded into a quartz optical vacuum chamber and cooled down by a cryocooler (CRYOMECH OptistatAC-V12W CP830). A wavelength of 325 nm helium–Cadmium laser from Kimmon was employed to excite crystal. The laser power density irradiated on the surface of crystals was about 320mw/cm².

3. Results and discussion

Fig. 1 shows the powder X-ray diffraction (XRD) pattern of $\text{CH}_3\text{NH}_3\text{PbBr}_{0.3}\text{Cl}_{2.7}$ and $\text{CH}_3\text{NH}_3\text{PbCl}_3$ powder. The main XRD peaks locating at around 15.44°, 21.84°, 31.20° and 34.88° are ascribed to (100), (110), (200) and (210), respectively. All these peaks indicate that $\text{CH}_3\text{NH}_3\text{PbCl}_3$ and $\text{CH}_3\text{NH}_3\text{PbBr}_{0.3}\text{Cl}_{2.7}$ perovskite crystals belong to cubic system with space group $\text{Pm}\bar{3}m$ [19]. According to Bragg's Law, interplanar spacing d could be calculated with the following equation:

$$2d \sin \theta = n\lambda \quad (1)$$

where d is the interplanar spacing, θ is the angle between the

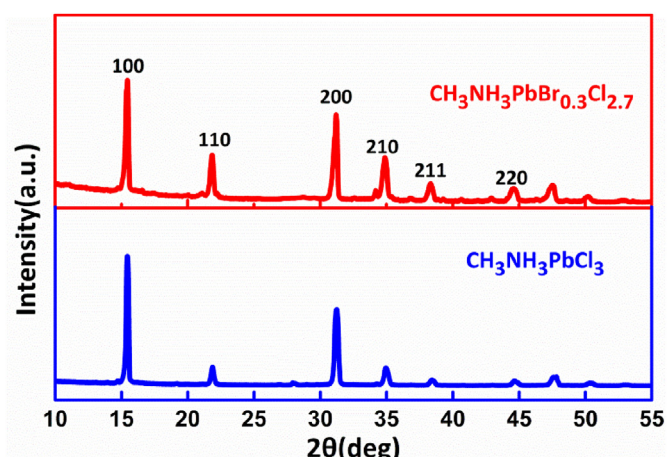


Fig. 1. XRD pattern of $\text{CH}_3\text{NH}_3\text{PbBr}_{0.3}\text{Cl}_{2.7}$ and $\text{CH}_3\text{NH}_3\text{PbCl}_3$ single crystals powder.

incident X-ray and the corresponding crystal plane, λ is the wavelength of the X-ray ($\text{Cu K}_\alpha \lambda = 0.1542 \text{ nm}$), and n is the number of reflections. The lattice parameters can be obtained by:

$$d = \frac{a}{\sqrt{h^2 + k^2 + l^2}} \quad (2)$$

Where h, k, l is the Miller index. The calculated lattice parameter value of $\text{CH}_3\text{NH}_3\text{PbCl}_3$ and $\text{CH}_3\text{NH}_3\text{PbBr}_{0.3}\text{Cl}_{2.7}$ are 5.743 \AA and 5.752 \AA , respectively. These results are consistent with previous reports [19–22]. The slightly increased lattice parameter after Br doped into $\text{CH}_3\text{NH}_3\text{PbCl}_3$ materials is mainly due to the atomic radius of Br is larger than Cl, which also induced the diffraction peaks shifting to lower angles. According to Vegard's law, the actual molar ratio between Br to Cl can be calculated to be about 0.3:2.7 based on the shift of the diffraction peak [14,23].

An X-ray fluorescence (XRF) system has been employed to measure the actual molar ratio of Br to Cl, as shown in Fig. 2. The XRF spectra was excited by X-ray tube with Mo target that operated at 25 kV. The peaks at the energy of 10.55 KeV, 12.61 KeV, and 14.76 KeV are attributed to the signal from $\text{L}\alpha_1$, $\text{L}\beta_1$, $\text{L}\gamma_1$ of Pb, respectively. The other two peaks locating at around 2.62 KeV and 11.88 KeV are ascribed to K_α peak of Cl and $\text{K}_{\alpha 2}$ peak of Br, respectively. The actual molar ratio between Br and Cl is 0.3:2.7, which is also consistent with the theoretical calculated value from XRD pattern. The other peaks are come from air or background shielding materials.

Fig. 3a shows transmission spectra of $\text{CH}_3\text{NH}_3\text{PbCl}_3$ and $\text{CH}_3\text{NH}_3\text{PbBr}_{0.3}\text{Cl}_{2.7}$ single crystals in the range from 350 nm to 600 nm. The crystals exhibit high transparency in the visible range up to 90% for $\text{CH}_3\text{NH}_3\text{PbCl}_3$ SCs. The transmission greatly drops to 40%, while Br doped into the pure $\text{CH}_3\text{NH}_3\text{PbCl}_3$ SCs. In addition, the sharp cut-off edge shifts to a longer wavelength with the doped Br. All these phenomena are ascribed to the optical band-gap change due to doped Br. We calculated the optical band-gap using Tauc's equation [24]:

$$\alpha h\nu = A(h\nu - E_g)^{\frac{1}{2}} \quad (3)$$

where α is the optical absorption coefficient; $h\nu$ is the energy of the incident photon; E_g is the optical band gap; and A is an energy-independent constant. The calculated optical band-gap can be obtained from x-intercept of the line tangent, as shown in Fig. 3b. The optical band-gap is shifted from 2.93 eV to 3.1 eV, which is ascribed to Br atom replacing the position of the Cl atom in the crystal

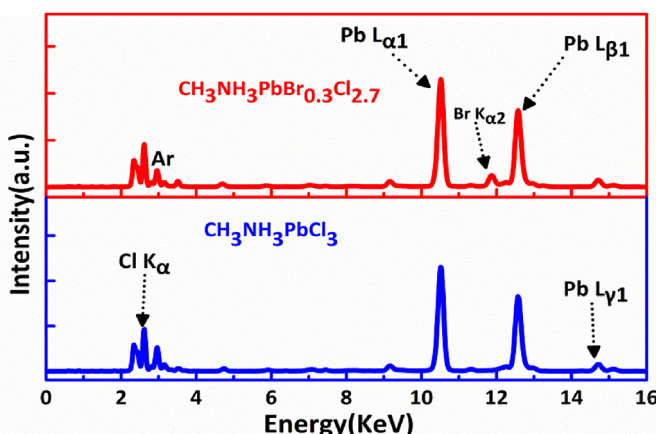


Fig. 2. X-ray fluorescence spectra of $\text{CH}_3\text{NH}_3\text{PbBr}_{0.3}\text{Cl}_{2.7}$ and $\text{CH}_3\text{NH}_3\text{PbCl}_3$ single crystals.

structure. These results are also consistent with previous reports [25–27].

In order to explore the effect of Br doping into $\text{CH}_3\text{NH}_3\text{PbCl}_3$ SCs, we have investigated the temperature-dependent PL spectra of $\text{CH}_3\text{NH}_3\text{PbCl}_3$ and $\text{CH}_3\text{NH}_3\text{PbBr}_{0.3}\text{Cl}_{2.7}$ SCs perovskites, respectively. During the measurement, the samples were placed in a vacuum chamber and excited by a laser with a wavelength of 325 nm. As shown in Fig. 4a and b, temperature-dependent PL spectra in the range of 350 nm–500 nm between 10 K and 290 K have been obtained. For $\text{CH}_3\text{NH}_3\text{PbCl}_3$ SCs (Fig. 4a), while the temperature is lower than 120 K, three typical distinct peaks centered at around 387 nm (labeled peak 1), 400 nm (labeled peak 2) and 415 nm (labeled peak 3) have been observed. As its a band-to-band direct semiconductor material, high energy peak 1 is ascribed to free exciton recombination emission, peak 2 is originated from the near bound exciton emission, the weak peak 3 is caused by the excitonic transition [28–32]. Both Peak 1 and 3 are disappeared at around 140 K–180 K. While for $\text{CH}_3\text{NH}_3\text{PbBr}_{0.3}\text{Cl}_{2.7}$ perovskite SCs (Fig. 4b), a single peak is presented. High energy peak 1^* is due to free exciton recombination emission, while the temperature is below 140 K. Low energy peak 2^* is ascribed to bound exciton recombination emission, while temperature is above 140 K. It is worth to be noticed that both high energy peak (1 and 1^*) and low energy peak (2 and 2^*) are existing at the temperature around 140 K, which is originated from a tetragonal structure [33]. These phenomena indicate that free exciton recombination emission is mainly contributed to PL spectra at orthorhombic structure, and bound exciton recombination emission is the dominated emission at cubic structure. The similar phenomenon has also been observed from solution growth organic or inorganic perovskite materials [34].

Furthermore, the emission peak energy and the FWHM of the two samples at different temperatures are plotted in Fig. 4c, d. The energy between free exciton recombination emission and bound recombination emission is about 76 meV and 130 meV for $\text{CH}_3\text{NH}_3\text{PbCl}_3$ and $\text{CH}_3\text{NH}_3\text{PbBr}_{0.3}\text{Cl}_{2.7}$, respectively. It is worth mentioning that electron-phonon interaction could cause PL emission blue shift, while at the same time, temperature increasing induced lattice expansion could cause PL emission red shift [35,36]. This typical phenomenon has been observed in lead composite semiconductors [28,29,37]. The band-gap changes at various temperatures can be estimated according to the following equation [36–38]:

$$E_g(T) = E_0 - \frac{\alpha T^2}{(T + \beta)} \quad (4)$$

Where α and β are fitting parameters characteristic of a given material, T is the temperature. According to this equation, the band-gap exhibits nonlinear decreasing trend at low temperature. While at relative high temperature, the decreasing trend tends to be linear. Interestingly, in Fig. 4c, slightly blue shift peak shifts under 140 K have been observed, mainly due to electron-phonon interaction is greater than the effect of lattice expansion and dominates below 140 K in $\text{CH}_3\text{NH}_3\text{PbCl}_3$. But the influence of the lattice expansion exceeds the contribution of the electron-phonon interaction above 140 K. Compared to Fig. 4d, peak red shifts in $\text{CH}_3\text{NH}_3\text{PbBr}_{0.3}\text{Cl}_{2.7}$ is more pronounced than $\text{CH}_3\text{NH}_3\text{PbCl}_3$ as the temperature increases, which may be attributed to the reduced bond energy in the lattice structure after Br doping into $\text{CH}_3\text{NH}_3\text{PbCl}_3$ SCs, so the lattice expansion is more sensitive to temperature changes. As a result, the final PL emission shift is balanced by the lattice expansion and the electron-phonon interaction, which varies at different temperature [39,40].

Since the orthorhombic phase is stable between 10 and 140 K for $\text{CH}_3\text{NH}_3\text{PbCl}_3$ and $\text{CH}_3\text{NH}_3\text{PbBr}_{0.3}\text{Cl}_{2.7}$, the exciton binding energy

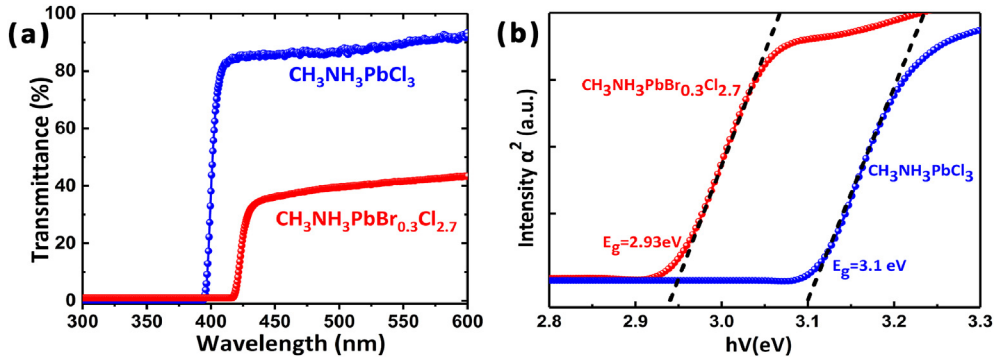


Fig. 3. (a) Optical transmission spectra of $\text{CH}_3\text{NH}_3\text{PbBr}_{0.3}\text{Cl}_{2.7}$ and $\text{CH}_3\text{NH}_3\text{PbCl}_3$ single crystals; (b) calculated optical band-gap of $\text{CH}_3\text{NH}_3\text{PbBr}_{0.3}\text{Cl}_{2.7}$ and $\text{CH}_3\text{NH}_3\text{PbCl}_3$ single crystals.

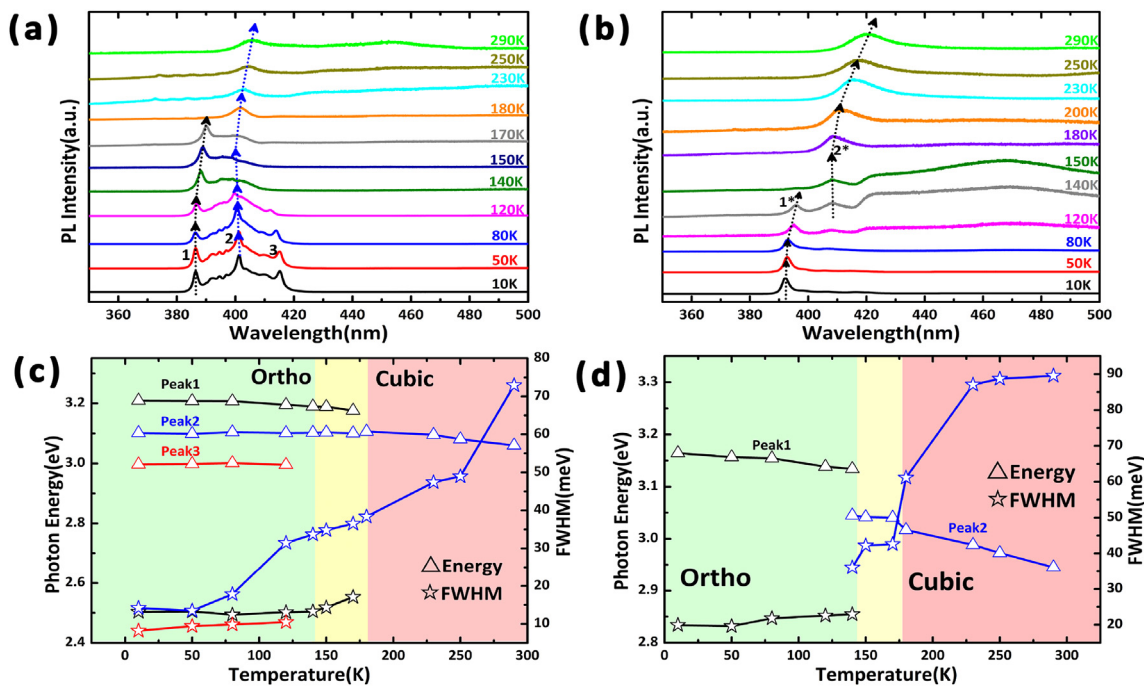


Fig. 4. (a, b) Temperature-dependent photoluminescence spectra, (c) and (d) Positions and FWHM of the labeled peaks, shown as a curve of temperature.

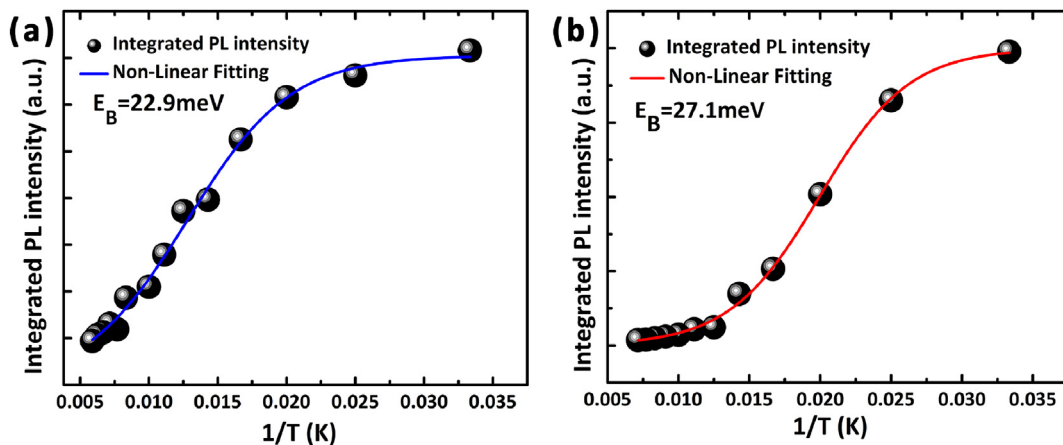


Fig. 5. (a,b) Temperature dependent data of integrated intensity of $\text{CH}_3\text{NH}_3\text{PbCl}_3$ and $\text{CH}_3\text{NH}_3\text{PbBr}_{0.3}\text{Cl}_{2.7}$ single crystals, respectively. The solid lines are fittings.

can be calculated from the temperature-dependent PL spectra, as shown in Fig. 5a and b. The relationship between light emission intensity and temperature is as follows [41–43]:

$$I(T) = \frac{I_0}{1 + Ae^{-E_B/k_B T}} \quad (5)$$

where $I(T)$ is the PL intensity, T is temperature, I_0 is the PL intensity at 0 K, E_B the exciton binding energy, and k_B the Boltzmann constant, and A is a fitting parameter. The fitted exciton binding energy of $\text{CH}_3\text{NH}_3\text{PbCl}_3$ and $\text{CH}_3\text{NH}_3\text{PbBr}_{0.3}\text{Cl}_{2.7}$ crystals are 22.9 meV and 27.1 meV, respectively. The results indicate that Br doped $\text{CH}_3\text{NH}_3\text{PbCl}_3$ materials are expected to increase the value of excitation binding energy. Unlike previously reported, the exciton binding energy value of $\text{CH}_3\text{NH}_3\text{PbCl}_3$ material is about 40 meV [44]. This is because the exciton characteristics of hybrid perovskites are correlated with the synthesis, composition and structure details [43].

4. Conclusions

In this article, we have grown high quality $\text{CH}_3\text{NH}_3\text{PbCl}_3$ and $\text{CH}_3\text{NH}_3\text{PbBr}_{0.3}\text{Cl}_{2.7}$ single crystals and investigated their structural and optical properties. XRD and XRF data demonstrated the crystal structure and the Br dopant concentration of the materials. Temperature-dependent PL spectra not only reveal the light emission properties from the orthorhombic-tetragonal-cubic phase transition, but also demonstrate free exciton recombination emission is mainly contributed to PL spectra at orthorhombic structure, and bound exciton recombination emission is the dominated emission at cubic structure. The calculated exciton binding energy of $\text{CH}_3\text{NH}_3\text{PbCl}_3$ and $\text{CH}_3\text{NH}_3\text{PbBr}_{0.3}\text{Cl}_{2.7}$ crystals are about 22.9 meV and 27.1 meV, respectively. These results reveal the fundamental mechanism of light emission for $\text{CH}_3\text{NH}_3\text{PbCl}_3$ and $\text{CH}_3\text{NH}_3\text{PbBr}_{0.3}\text{Cl}_{2.7}$, and promote their future applications in optoelectronic devices.

Acknowledgements

This work was funded by the National Natural Science Foundation of China (Grants No. 11705090, 11875166, and 11435010). Prof. Tang acknowledge the supported by the National Natural Science Foundation of China (Grant No. 11690040, 11690043). The authors acknowledge Dr. Hongying Yang for her expert assistance for further discussion and language polishing.

References

- [1] N.J. Jeon, H. Na, E.H. Jung, T.Y. Yang, Y.G. Lee, G. Kim, H.W. Shin, S.I. Seok, J. Lee, J. Seo, A fluorene-terminated hole-transporting material for highly efficient and stable perovskite solar cells, *Nat. Energy* 3 (2018) 682–689.
- [2] A. Dubey, N. Adhikari, S. Mabrouk, F. Wu, K. Chen, S. Yang, Q. Qiao, A strategic review on processing routes towards highly efficient perovskite solar cells, *J. Mater. Chem. A* 6 (2018) 2406–2431.
- [3] Y. Fang, Q. Dong, Y. Shao, Y. Yuan, J. Huang, Highly narrowband perovskite single-crystal photodetectors enabled by surface-charge recombination, *Nat. Photon.* 9 (2015) 679–686.
- [4] L. Zhao, K.M. Lee, K. Roh, S.U.Z. Khan, B.P. Rand, Improved outcoupling efficiency and stability of perovskite light-emitting diodes using thin emitting layers, *Adv. Mater.* 31 (2019) 1805836.
- [5] J. Miao, F. Zhang, Recent progress on highly sensitive perovskite photodetectors, *J. Mater. Chem. C* 7 (2019) 1741–1791.
- [6] W. Yu, F. Li, L. Yu, M.R. Niazi, Y. Zou, D. Corzo, A. Basu, C. Ma, S. Dey, M.L. Tietze, U. Buttner, X. Wang, Z. Wang, M.N. Hedhili, C. Guo, T. Wu, A. Amassian, Single crystal hybrid perovskite field-effect transistors, *Nat. Commun.* 9 (2018) 5354.
- [7] H. Wei, J. Huang, Halide lead perovskites for ionizing radiation detection, *Nat. Commun.* 10 (2019) 1066.
- [8] S. Yakunin, M. Sytnyk, D. Kriegner, S. Shrestha, M. Richter, G.J. Matt, H. Azimi, C.J. Brabec, J. Stangl, M.V. Kovalenko, W. Heiss, Detection of X-ray photons by solution-processed lead halide perovskites, *Nat. Photon.* 9 (2015) 444–449.
- [9] W. Wei, Y. Zhang, Q. Xu, H. Wei, Y. Fang, Q. Wang, Y. Deng, T. Li, A. Gruber, L. Cao, J. Huang, Monolithic integration of hybrid perovskite single crystals with heterogenous substrate for highly sensitive X-ray imaging, *Nat. Photon.* 11 (2017) 315–321.
- [10] Q. Xu, H. Wei, W. Wei, W. Chuirazzi, D. DeSantis, J. Huang, L. Cao, Detection of charged particles with a methylammonium lead tribromide perovskite single crystal, *Nucl. Instrum. Methods Phys. Res. A* 848 (2017) 106–108.
- [11] V. Pawar, M. Kumar, P.A. Jha, S.K. Gupta, P.K. Jha, P. Singh, Cs/MAPbI₃ composite formation and its influence on optical properties, *J. Alloys Compd.* 783 (2019) 935–942.
- [12] B. Zong, W. Fu, H. Liu, L. Huang, H. Bala, X. Wang, G. Sun, J. Cao, Z. Zhang, Highly stable hole-conductor-free $\text{CH}_3\text{NH}_3\text{Pb}(\text{I}-x\text{Br})_3$ perovskite solar cells with carbon counter electrode, *J. Alloys Compd.* 748 (2018) 1006–1012.
- [13] G. Qiao, Z. Zeng, J. Gao, Y. Tang, Q. Wang, An efficient route to assemble novel organometal halide perovskites and emission evolution performance, *J. Alloys Compd.* 771 (2019) 418–423.
- [14] H. Wei, D. DeSantis, W. Wei, Y. Deng, D. Guo, T.J. Savenije, L. Cao, J. Huang, Dopant compensation in alloyed $\text{CH}_3\text{NH}_3\text{PbBr}_3-x\text{Cl}_x$ perovskite single crystals for gamma-ray spectroscopy, *Nat. Photon.* 16 (2017) 826–833.
- [15] Q. Chen, H. Zhou, Y. Fang, A.Z. Stieg, T.B. Song, H.H. Wang, X. Xu, Y. Liu, S. Lu, J. You, P. Sun, J. McKay, M.S. Goorsky, Y. Yang, The optoelectronic role of chlorine in $\text{CH}_3\text{NH}_3\text{PbI}_3(\text{Cl})$ -based perovskite solar cells, *Nat. Commun.* 6 (2015) 7269.
- [16] W. Wu, X. Wang, X. Han, Z. Yang, G. Gao, Y. Zhang, J. Hu, Y. Tan, A. Pan, C. Pan, Flexible photodetector arrays based on patterned $\text{ch}_3\text{nh}_3\text{pb}_3\text{i}-x\text{cl}_x$ perovskite film for real-time photosensing and imaging, *Adv. Mater.* 31 (2019) 1805913.
- [17] J. Hieulle, X. Wang, C. Stecker, D.Y. Son, L. Qiu, R. Ohmann, L.K. Ono, A. Mugarza, Y. Yan, Y. Qi, Unraveling the impact of halide mixing on perovskite stability, *J. Am. Chem. Soc.* 141 (2019) 3515–3523.
- [18] Q. Shan, X. Zhang, Y. Zhang, W. Jia, Y. Ling, D. Hei, S. Chu, Development of an online X-ray fluorescence analysis system for heavy metals measurement in cereal raw meal, *Spectrosc. Lett.* 49 (2016) 188–193.
- [19] Y. Liu, Z. Yang, D. Cui, X. Ren, J. Sun, X. Liu, J. Zhang, Q. Wei, H. Fan, F. Yu, X. Zhang, C. Zhao, S. (Frank) Liu, Two-Inch-Sized perovskite $\text{CH}_3\text{NH}_3\text{PbX}_3$ ($X = \text{Cl}, \text{Br}, \text{I}$) crystals: growth and characterization, *Adv. Mater.* 27 (2015) 5176–5183.
- [20] T. Zhang, M. Yang, E.E. Benson, Z. Li, J.V.D. Lagemaat, J.M. Luther, Y. Yan, K. Zhu, Y. Zhao, A facile solvothermal growth of single crystal mixed halide perovskite $\text{CH}_3\text{NH}_3\text{Pb}(\text{Br}_1-x\text{Cl}_x)_3$, *Chem. Commun.* 51 (2015) 7820–7823.
- [21] E. Zheng, B. Yuh, G.A. Tosado, Q. Yu, Solution-processed visible-blind UV-A photodetectors based on $\text{CH}_3\text{NH}_3\text{PbCl}_3$ perovskite thin films, *J. Mater. Chem. C* 5 (2017) 3796–3806.
- [22] M. Zhang, H. Yu, M. Lyu, Q. Wang, J.H. Yun, L. Wang, Composition-dependent photoluminescence intensity and prolonged recombination lifetime of perovskite $\text{CH}_3\text{NH}_3\text{PbBr}_3-x\text{Cl}_x$ films, *Chem. Commun.* 50 (2014) 11727–11730.
- [23] J.H. Noh, S.H. Im, J.H. Heo, T.N. Mandal, S. Seok, Chemical management for colorful, efficient, and stable inorganic–organic hybrid nanostructured solar cells, *Nano Lett.* 13 (2013) 1764–1769.
- [24] Z. Zhang, L. Ren, H. Yan, S. Guo, S. Wang, M. Wang, K. Jin, Bandgap narrowing in Bi-doped $\text{CH}_3\text{NH}_3\text{PbCl}_3$ perovskite single crystals and thin films, *J. Phys. Chem. C* 121 (2017) 17436–17441.
- [25] A. Sadhanala, S. Ahmad, B. Zhao, N. Giesbrecht, P.M. Pearce, F. Deschler, R.L.Z. Hoye, K.C. Gödel, T. Bein, P. Docampo, S.E. Dutton, M.F.L. De Volder, R.H. Friend, Blue-Green color tunable solution processable organolead chloride–bromide mixed halide perovskites for optoelectronic applications, *Nano Lett.* 15 (2015) 6095–6101.
- [26] K.T. Butler, J.M. Frost, A. Walsh, Band alignment of the hybrid halide perovskites $\text{CH}_3\text{NH}_3\text{PbCl}_3$, $\text{CH}_3\text{NH}_3\text{PbBr}_3$ and $\text{CH}_3\text{NH}_3\text{PbI}_3$, *Mater. Horiz.* 2 (2015) 228.
- [27] N.K. Kumawat, A. Dey, A. Kumar, S.P. Gopinathan, K.L. Narasimhan, Dinesh Kabra, Band gap tuning of $\text{CH}_3\text{NH}_3\text{Pb}(\text{Br}_1-x\text{Cl}_x)_3$ hybrid perovskite for blue electroluminescence, *ACS Appl. Mater. Interfaces* 7 (2015) 13119–13124.
- [28] V. D'Innocenzo, G. Grancini, M.J.P. Alcocer, A.R.S. Kandada, S.D. Stranks, M.M. Lee, G. Lanzani, H.J. Snaith, A. Petrozza, Excitons versus free charges in organic-lead tri-halide perovskites, *Nat. Commun.* 5 (2014) 3586.
- [29] H. Fang, R. Raissa, M. Abdu-Aguye, S. Adjokatse, G.R. Blake, J. Even, M.A. Loi, Photophysics of organic–inorganic hybrid lead iodide perovskite single crystals, *Adv. Funct. Mater.* 25 (2015) 2378–2385.
- [30] J. Xing, X. Liu, Q. Zhang, S.T. Ha, Y. Yuan, C. Shen, T.C. Sum, Q. Xiong, Vapor phase synthesis of organometal halide perovskite nanowires for tunable room-temperature nanolasers, *Nano Lett.* 15 (2015) 4571–4577.
- [31] C. Wehrenfennig, M. Liu, H.J. Snaith, M.B. Johnston, L.M. Herz, Charge carrier recombination channels in the low-temperature phase of organic inorganic lead halide perovskite thin films, *Apl. Mater.* 2 (2014), 081513.
- [32] J. Dai, H. Zheng, C. Zhu, J. Luc, C. Xu, Comparative investigation on temperature dependent photoluminescence of $\text{CH}_3\text{NH}_3\text{PbBr}_3$ and $\text{CH}(\text{NH}_2)_2\text{PbBr}_3$ microstructures, *J. Mater. Chem. C* 4 (2016) 4408–4413.
- [33] A. Poglitsch, D. Weber, Dynamic disorder in methylammonium-nium-trihalogenoplumbates (II) observed by millimeter wave spectroscopy, *J. Chem. Phys.* 87 (1987) 6373–6378.
- [34] J. Li, X. Yuan, P. Jing, J. Li, M. Wei, J. Hua, J. Zhao, L. Tian, Temperature-dependent photoluminescence of inorganic perovskite nanocrystal films, *RSC Adv.* 6 (2016) 78311–78316.

- [35] H. Linnenbank, M. Saliba, L. Gui, B. Metzger, S.G. Tikhodeev, J. Kadro, G. Nasti, A. Abate, A. Hagfeldt, M. Graetzel, H. Giessen, Temperature dependent two-photon photoluminescence of $\text{CH}_3\text{NH}_3\text{PbBr}_3$: structural phase and exciton to free carrier transition, *Opt. Mater. Express* 8 (2018) 511–521.
- [36] Y.P. Varshni, Temperature dependence of the energy gap in semiconductors, *Physica* 34 (1967) 149–154.
- [37] G. Rainò, G. Nedelcu, L. Protesescu, M.I. Bodnarchuk, M.V. Kovalenko, R.F. Mahrt, T. Stöferle, Single cesium lead halide perovskite nanocrystals at low temperature: fast single-photon emission, reduced blinking, and exciton fine structure, *ACS Nano* 10 (2016) 2485–2490.
- [38] K.P. O'Donnell, X. Chen, Temperature dependence of semiconductor band gaps, *Appl. Phys. Lett.* 58 (1991) 2924–2926.
- [39] Q. Dai, Y. Zhang, Y. Wang, M.Z. Hu, B. Zou, Y. Wang, W.W. Yu, Size-dependent temperature effects on PbSe nanocrystals, *Langmuir* 26 (2010) 11435–11440.
- [40] K. Wei, Z. Xu, R. Chen, X. Zheng, X. Cheng, T. Jiang, Temperature-dependent excitonic photoluminescence excited by two-photon absorption in perovskite CsPbBr_3 quantum dots, *Opt. Lett.* 41 (2016) 3821–3824.
- [41] T.J. Savenije, C.S. Ponceca, L. Kunnenman, M. Abdellah, K. Zheng, Y. Tian, Q. Zhu, S.E. Canton, I.G. Scheblykin, T. Pullerits, A. Yartsev, V. Sundstrom, Thermally activated exciton dissociation and recombination control the carrier dynamics in organometal halide perovskite, *J. Phys. Chem. Lett.* 5 (2014) 2189–2194.
- [42] X. Sun, Z. Shi, Y. Li, L. Lei, S. Li, D. Wu, T. Xu, Y. Tian, X. Li, Effect of $\text{CH}_3\text{NH}_3\text{I}$ concentration on the physical properties of solution processed organometal halide perovskite $\text{CH}_3\text{NH}_3\text{PbI}_3$, *J. Alloys Compd.* 706 (2017) 274–279.
- [43] K. Wu, A. Bera, C. Ma, Y. Du, Y. Yang, L. Lib, T. Wu, Temperature-dependent excitonic photoluminescence of hybrid organometal halide perovskite films, *Phys. Chem. Chem. Phys.* 16 (2014) 22476–22481.
- [44] T. Yamada, T. Aharen, Y. Kanemitsu, Near-band-edge optical responses of $\text{CH}_3\text{NH}_3\text{PbCl}_3$ single crystals: photon recycling of excitonic luminescence, *Phys. Rev. Lett.* 120 (2018), 057404.